X-ray reciprocal space maps and x-ray scattering topographic observation of GaN layer on GaAs (001) in plasma-assisted molecular beam epitaxy

Yoshifumi Suzuki,[a] Masakazu Shinbara, Hideki Kii, and Yoshinori Chikaura
Graduate School of Engineering, Kyushu Institute of Technology, Kitakyushu 804-8550, Japan

(Received 14 November 2006; accepted 19 January 2007; published online 21 March 2007)

We have characterized plasma-assisted N^+ molecular beam epitaxy-grown polymorphous GaN epitaxial layer on GaAs by x-ray reciprocal mapping using four-circle x-ray diffractometer and a personal computer controlled x-ray scattering topography system by ourselves. x-ray reciprocal mapping indicates that GaN wurtzite epitaxial film was grown along only $[\bar{1}\bar{1}1]$ direction. While GaN wurtzite and zinc-blende crystals were contracted along the surface normal, those of lattice constants were expanded along lateral direction. The values of expansion were larger than our instrumental resolution. The lateral expansion rate of lattice constants in GaN wurtzite was larger than that in GaN zinc blende. It was found that zinc-blende phase was unevenly distributed, but wurtzite one was uniformly distributed by growth condition. © *2007 American Institute of Physics*. [DOI: 10.1063/1.2712166]

I. INTRODUCTION

Recently, high-brightness blue LEDs based on GaN have become commercially available, and have been investigated by a number of research groups as a potential material system for shorter wavelength optical devices.[1–3] However, it has not been easy to grow epitaxial layers, because there are no adequate substrates for lattice matching and it is very difficult to obtain epitaxial layer with good crystal quality. Moreover, it seems that the hexagonal (wurtzite) phase often coexists with cubic (zinc-blende) one. It is indicated by Ref. 4 that standard ω-2θ x-ray diffraction scans measure only the lattice spacing parallel to the film surface and therefore cannot distinguish between the zinc-blende and wurtzite polymorphs if they have one of the above orientations. X-ray reciprocal space maps have been capable for detecting the wurtzite GaN domains oriented $[0001]\|[111]$ As.[5]

Self-assembly in semiconductor nanostructures is a strategy for nanofabrication that involves designing each individual atom or molecule entities so that shape-complementary causes them to aggregate into desired structures. Self-assembly has a number of advantages as a strategy: First, it carries out many of the most difficult steps in nanofabrication—those involving atomic-level modification of structure—using the very highly developed techniques of synthetic chemistry. Second, because it requires that the target structures be the thermodynamically most stable ones open to the system, it tends to produce structures that are relatively defect-free and self-healing. Systematic variations in the compositional modulation due to the structural design and the growth conditions of the superlattice are characterized by routine mapping of the lateral satellites. It is possible to obtain a complete analysis of a complex semiconductor layer structure (which is very closely related to electrical properties). The power of reciprocal-space mapping in two dimensions arises in a singular way: by breaking the perfect in-plane homogeneity of the layered epitaxial single crystal through the introduction of lateral structure. Consider first a laterally perfect crystal comprised of individual lamellae that are each laterally homogenous; all structural variations occur normal to the lamellae; an example would be an ideally coherent conventional superlattice grown on a singular substrate. In order to study self-assembly in semiconductor nanostructures, we should characterize epitaxial films concerned to structure correlation to crystal conditions, for example, for two polymorphs (wurtzite and zinc-blende structures) if they have one of the above orientation.

The aim of this paper is demonstration of characterization for a GaN epitaxial layer grown by plasma-assisted molecular beam epitaxy on GaAs (001) substrate using four circle x-ray diffractometer with four axes omega, 2theta, chi, phi. And a topography study was performed for the sample, the GaN epitaxial layer and the GaAs (001) substrate, concerned with between wurtzite and zinc-blende structures, two-polymorphs states. The results gave a valuable suggestion of correlation for more sensitive crystal growth of zinc blende than that of wurtzite.

II. EXPERIMENTS

A. Sample

Growth on epitaxial GaN film is carried out on (001)-oriented (offcut $<0.1°$), semi-insulating GaAs substrate in a custom-designed solid-source molecular beam epitaxy (MBE) chamber. Active N is generated by a high voltage ($\simeq$1.5 keV) plasma glow discharge. The plasma power is kept for all growth procedure at 30 W. During epitaxial growth we can change the growth conditions, and in spite of constant growth condition there are possibilities with changing the crystal quality. The surface of the growing crystal is monitored *in situ* by reflection high-energy electron diffraction. The detailed growth condition was described in Ref. 5.

[a]Electronic mail: ysuzuki@e-lab.kyutech.ac.jp

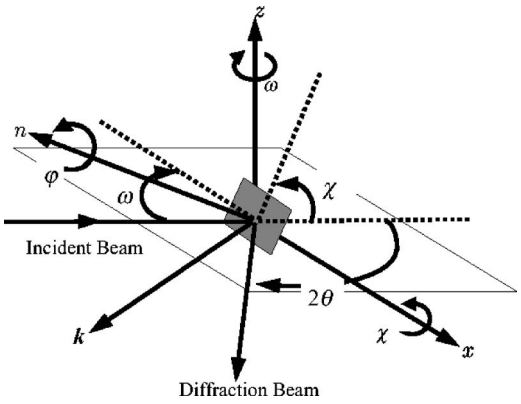

FIG. 1. Schematic representation of the four-circle geometry.

A sample used in this work is a GaN epitaxial layer (500 nm).

B. Reciprocal lattice space mapping

Reciprocal lattice space mapping measurements are performed with structure analysis diffractometer (RASA-7R, Rigaku Co.), which have an Eulerian cradle four-circle $(\varphi,\chi,\omega,2\theta)$ diffractometer (as shown in Fig. 1) allowing access to a large volume of reciprocal space. An x-ray source is monochromatized with graphite (0002) plate ($12\times12\times2$ mm^3) monochromator crystal and collimator (0.3 mm ϕ), and employing Cu $K\alpha_1$ (wavelength λ is 1.5405 Å) radiation from a rotating anode (50 kV/150 mA). The system is originally designed to structural analysis for single crystal with automated four-circle control and data collection software (AFC, Rigaku Co.). So, we changed the software program in order to fit to the present reciprocal lattice space mapping measurement. A schematic of the four-circle geometry is shown in Fig. 1. The horizontal plane H is defined by the incident and diffracted beams; χ is defined as the angle between the sample surface and plane H and $\chi=0$ when they are paralel. At $\chi=90°$ [001] direction is parallel to diffraction vector **g**. The x-ray reciprocal space maps of symmetric Bragg reflection measurements are performed using ω-2θ coupling scan mode at a certain plane, by changing χ step by step. Consequently 2-dimensional intensity maps $I(2\theta/2,\chi)$ are obtained at $\varphi=0°$, ±90°, and 180°, where the angle φ measures the rotation around the surface normal of the substrate. $I(2\theta/2,\chi)$ $[=I(\omega,\chi)]$ maps are not represented with reciprocal lattice space. The relationships between (ω,χ) in Eulerian diffractometer and the reciprocal space coordinates $(Q_x,Q_z)=(1/d_{hh0},1/d_{00l})$ is given by Eqs. (1) and (2),

$$\frac{1}{d_{hh0}}=\frac{2}{\lambda}\sin\omega\cos\chi, \tag{1}$$

$$\frac{1}{d_{00l}}=\frac{2}{\lambda}\sin\omega\sin\chi \tag{2}$$

However, we can easily transform from $I(\omega,\chi)$ to $I'(1/d_{hh0},1/d_{00l})$; it does not represent a picture,

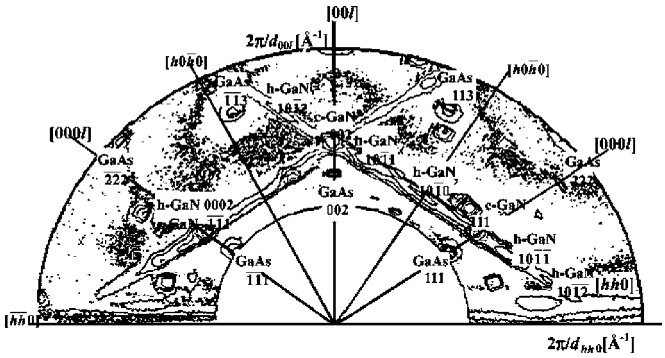

FIG. 2. X-ray reciprocal space map at $\varphi=0°$.

$$I'(i,j)=I(\chi_m,\omega_n)(1-p)(1-q)+I(\chi_{m+1},\omega_n)p(1-q)+I(\chi_m,\omega_{n+1})(1-p)q+I(\chi_{m+1},\omega_{n+1})pq,$$

$$p=i-m,\quad q=j-n. \tag{3}$$

Using linear interpolation algorithm as reference equation (3), we can obtain $I(i,j)$ intensity distribution.

C. X-ray scattering topography

An x-ray scattering topography system has been described in previous papers.[6–8] A personal computer controlled x-ray scattering topography system has finely collimated x-ray beam and the specimen, which can be rotated stepwise, is mechanically scanned with x-z two-dimensional translation. The intensity data are obtained and image processing is carried out using personal computers. The sample is placed in a front of a sealed-off cobalt x-ray tube (x-ray conditions: 40 kV/20 mA; fine focused 0.4×8 mm^2 to size) and employing Co $K\alpha_1$ (wavelength λ is 1.7889 Å) radiation, which is scanned with finely collimated x-ray beam (0.1 mm ϕ) using (004) and $(10\bar{1}1)$ symmetry reflection of zinc-blende GaN and symmetry reflection of wurtzite GaN, respectively. The $(10\bar{1}1)$ diffraction of wurtzite GaN is obtained utilizing a four-circle diffractometer, which has been constructed by ourselves. The schematic representation of the four-circle geometry shown in Fig. 1 coincided with the reciprocal lattice space mapping, but real apparatus is a different system. The horizontal plane H, angle χ, and angle φ are the same as described above. The 2θ is defined as the angle between the incident and diffracted beam and the angle ω measures the sample rotation around the axis perpendicular to the H plane. In wurtzite observation case, χ is not 90°, so that z translation axis does not coincide with $[00l]$ direction. Owing to the division, a topograph is deformed with parallel rectangular. A deformed topograph is reduced with affine transformation and linear interpolation method. The algorithm is expressed with the following equation:

$$\begin{pmatrix}x'\\z'\end{pmatrix}=\begin{pmatrix}1 & s_1\\ s_2 & 1\end{pmatrix}\begin{pmatrix}x\\z\end{pmatrix}. \tag{4}$$

s_1 and s_2 are amount of inclination for x and z directions, respectively. (x,z) is a coordinate before transformation; (x',z') is a coordinate after transformation. It is possible to approximate from the following equations the value of $I(i,j)$,

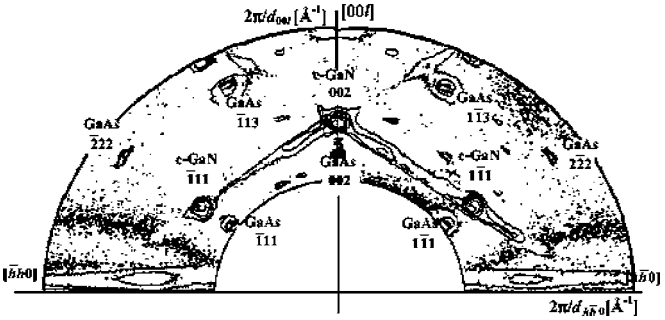

FIG. 3. X-ray reciprocal space map at $\varphi=90°$.

where (i,j) is no-cite point, using four lattice points (ξ,η), $(\xi,\eta+1)$, $(\xi+1,\eta)$, and $(\xi+1,\eta+1)$,

$$I'(i,j) = I(\xi,\eta)(1-p)(1-q) + I(\xi+1,\eta)p(1-q) + I(\xi,\eta+1)(1-p)q + I(\xi+1,\eta+1)pq, \quad (5)$$

where $p=i-\xi$ and $q=j-\eta$.

III. RESULTS AND DISCUSSION

A. Reciprocal lattice space mapping

The x-ray reciprocal lattice space maps, measurements for four symmetrical planes to sample along the $[00l]$ direction, $\varphi=0°$, ±90°, and 180°, were measured with $\omega-2\theta$ scan of 13°–32°; χ parameters were changed 0°–180° step by step. The relationships between $(2\theta/2, \chi)$ in reciprocal space coordinates $(1/d_{hh0}, 1/d_{00l})$ was given by Eqs. (1) and (2).

Figure 2 shows x-ray reciprocal space map at $\varphi=0°$, namely, $(1\bar{1}0)$ cross section. The map shows that there are both zinc-blende GaN represented with *c*-GaN and wurtzite GaN represented with *h*-GaN, and reflection indexes. As shown in this figure, in the left-hand side of the figure, $[hh0]$ direction, there are no $10\bar{1}1$, $10\bar{1}0$, $10\bar{1}\bar{1}$, and $10\bar{1}\bar{2}$; in the right-hand side of the figure, $[\bar{h}\bar{h}0]$ direction, there are no $10\bar{1}2$, and this indicates that the map is not symmetric about $[00l]$ axis. Moreover the wurtzite *h*-GaN 0002 and zinc-blende *c*-GaN $\bar{1}\bar{1}1$ reciprocal points are coincident with each other, and that of wurtzite *h*-GaN 0002 and zinc-blende *c*-GaN 111 do not coincide. It means that the *h*-GaN (0002) plane and zinc-blende $(\bar{1}\bar{1}1)$ stacking planes have the same lattice spacing. It indicates, on the other hand, that *h*-GaN (0002) plane does not stack on zinc blende (111).

TABLE I. The relative values of lattice constants expansion and contraction in GaN wurzite and zinc-blende epitaxial film and the relative values of lattice constants expansion and contraction in GaAs substrate.

	h-GaN	*c*-GaN
Growth direction	0.022%	0.051%
($\mathbf{a}_3$ or *c*)	Contraction	Contraction
Lateral direction	0.23%	0.018%
($\mathbf{a}_1$,$\mathbf{a}_2$)	0.29%	0.005%
	Expansion	Expansion
	GaAs	
Growth direction	0.095%	
	Expansion	
Lateral direction	0.012%	
	Contraction	

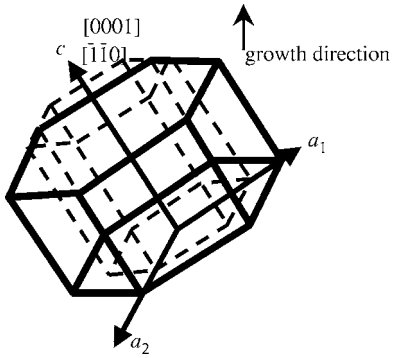

FIG. 4. A model of unit cell, for *h*-GaN wurtzite.

Figure 3 shows an x-ray reciprocal space map at $\varphi=90°$, namely, (110) cross section. The map shows that there are only zinc-blende GaN. We could not obtain clear coincidence of *h*-GaN $01\bar{1}0$, $0\bar{1}10$, and *c*-GaN $2\bar{2}0$, $\bar{2}20$, owing to angular low resolution for goniometer and beam divergence of x-ray source. It indicates that wurtzite GaN oriented such that only $[0001]\|[1\bar{1}1]$. Between GaN (002) and $(\bar{1}11)$ and $(1\bar{1}1)$, some peaks exist at points of 1/3 and 2/3. They are due to stacking faults or twins corresponding to ABCABC… and CBACBA… packing only to $\bar{1}11$ and $1\bar{1}1$.

The lattice deformations, growth orientation (*c*), and lateral orientation ($\mathbf{a}_1$, $\mathbf{a}_2$) were measured using x-ray reciprocal space mapping at $\varphi=0°$, 90°, and 45° $\omega-2\theta$ scanning. Higher angle 2θ was adopted in order to obtain higher resolution for lattice parameter values. It was used not only for growth orientation [001], but also for lateral direction [110] and $[1\bar{1}0]$ and measuring (0002) and $(10\bar{1}2)$ diffractions for wurtzite GaN, and (004), (222) ones for zinc-blende GaN, and (006), (222) GaAs substrate, and lattice constants of growth orientation and lateral direction. Table I summarizes the values of expansion and contraction in GaN wurtzite and zinc-blende polymorphous epitaxial film, and GaAs substrate. It is noted that *h*-GaN wurtzite was contracted along the growth direction, but that it was expanded for lateral direction. The tendency for *c*-GaN zinc blend was similar as *h*-GaN wurtzite. Comparing behavior of contractions and expansions between *h*-GaN wurtzite and *c*-GaN zinc blend, the values of contraction are similar. On the other hand, that of expansion in *h*-GaN wurtzite was larger than that in *c*-GaN

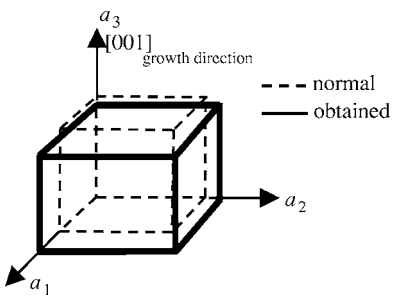

FIG. 5. A model of unit cell, for *c*-GaN zinc blende.

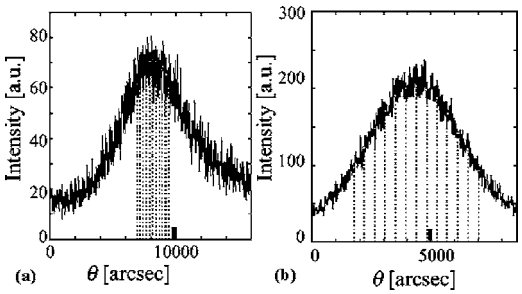

FIG. 6. ω-rocking curve of the epitaxial film. (a) for *c*-GaN zinc blende (004) and (b) for *h*-Ga*N* wurtzite $(10\bar{1}1)$ diffraction.

zinc blende, while GaAs substrate was expanded for growth direction $[00l]$ and was contracted in lateral direction $[hh0]$ and $[h\bar{h}0]$. The contraction of GaAs substrate was influenced from smaller lattice constants in epitaxial film of GaN, and consequently lattice constants in $[00l]$ direction for GaAs was expanded due to Poisson ratios. Summarizing the results as described above, Figs. 4 and 5 show models of unit cells for *h*-GaN wurtzite and *c*-GaN zinc blende, as shown in Figs. 4 and 5, respectively. It is found that *h*-GaN wurtzite unit cell was oriented along only $[\bar{1}\bar{1}1]$ As direction, namely, GaN wurtzite crystal grows only $[\bar{1}\bar{1}1]$ As direction.

B. X-ray scattering topography

Figures 6(a) and 6(b) show ω-rocking curve of the epitaxial film *c*-GaN zinc blende (004) and *h*-GaN wurtzite $(10\bar{1}1)$ diffraction, respectively. The (004) and $(10\bar{1}1)$ diffraction peaks have full width at half maxima (FWHMs) of 7700 and 4800 arc sec, respectively. The FWHM of zinc blende is wider, as shown in Fig. 2, than that of wurtzite.

Figure 7 shows *c*-GaN zinc blende (004) x-ray scattering topographs, of which incident direction was orthogonal to each other. They are obtained as similar images. Figures 8(a) and 8(b) show GaN $(10\bar{1}1)$ x-ray scattering topographs, of which (a) has not been corrected yet, and (b) has been carried out in affine transformation of Eq. (5) and linear interpolation procedure of Eqs. (6) and (7). In order to compare the amount of GaN wurtzite with zinc blende, we took integrated intensity x-ray scattering topographs. Figures 9(a) and 9(b)

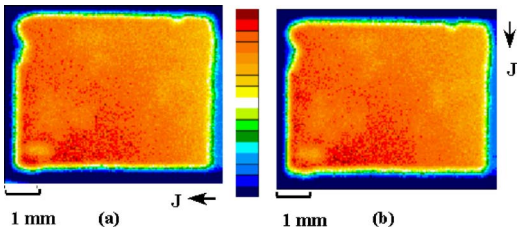

FIG. 7. (Color online) *c*-GaN zinc blende (004) x-ray scattering topographs, of which incident direction is orthogonal to each other.

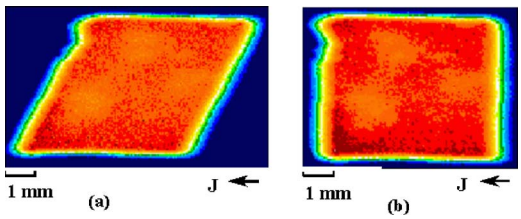

FIG. 8. (Color online) GaN $(10\bar{1}1)$ x-ray scattering topographs. (a) has not been corrected yet, and (b) has been carried out in affine transformation of Eq. (5) and linear interpolation procedure of Eqs. (6) and (7).

presented integrated intensity x-ray scattering topographs for GaN (004) and $(10\bar{1}1)$, respectively. An integrated intensity x-ray scattering topograph is a mapping of summation of intensities several x-ray scattering topographs, stepwise changing the ω angle. For example of Fig. 9(a) an integrated intensity x-ray scattering topograph, at a certain point of *x*-*z* site, is

$$I_{x-z} = \sum_{\omega=7000}^{9710} (\text{intensity})_{\omega}$$

[refer to Fig. 6(a)].

The integrated intensity map indicated the amount of crystal. Figure 9(a) means that in upper part of right-hand side GaN cubic phase is comparatively less. On the other hand, Fig. 9(b) indicates that GaN hexagonal phase exists thoroughly except for a few spots. Comparing to each other integrated intensity topographs, GaN-hexagonal phase exists is more dominant. It is suggested that the growth condition for *c*-GaN zinc blende is more sensitive than that for *h*-GaN wurtzite crystal. Namely, the results indicated that it is difficult to grow *c*-GaN zinc blende; however, Brandt *et al.*[5] described an approach for the *in situ* control of surface stoichiometry for the GaN on GaAs. They succeeded in growing pure *c*-GaN zinc blende on GaAs (001) substrates by the plasma-assisted MBE.

IV. CONCLUSION

We have characterized plasma-assisted N^+ MBE-grown polymorphous GaN epitaxial layer on GaAs by x-ray recip-

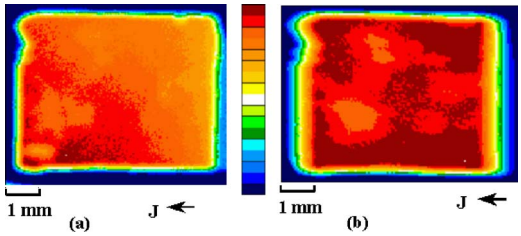

FIG. 9. (Color online) Integrated intensity x-ray scattering topographs (a) for *c*-GaN zinc blende (004) and (b) for *h*-GaN wurtzite $(10\bar{1}1)$, respectively.

rocal mapping and x-ray scattering topography to arrive at the following three conclusions:

(1) GaN wurtzite epitaxial film was grown along only the $[\bar{1}\bar{1}1]$ direction.
(2) While GaN wurtzite and zinc-blende crystals were contracted along the surface normal, those were expanded along the lateral direction which was larger than our instrumental resolution. The lateral expansion of lattice constants in GaN wurtzite was larger than that in GaN zinc blende.
(3) It was found that the zinc blende phase was unevenly distributed, but the wurtzite one was uniformly distributed by growth condition.

ACKNOWLEDGMENT

One of the authors (Y.S.) acknowledges the grant of Stiftung by Kyushu Institute of Technology, grant program of Paul Durude Institute.

[1] S. Strite, M. E. Lin, and H. Morcoc, Thin Solid Films **231**, 197 (1993).
[2] S. Nakamura, T. Mukai, and M. Senoh, Appl. Phys. Lett. **64**, 1687 (1994).
[3] S. D. Lester, F. A. Ponce, M. G. Craford, and D. A. Steigerwald, Appl. Phys. Lett. **66**, 1249 (1995).
[4] T. Lei and K. F. Ludwig, Jr., J. Appl. Phys. **74**, 4430 (1993).
[5] O. Brandt, H. Yang, B. Jenichen, Y. Suzuki, L. Däweritz, and H. Ploog, Phys. Rev. B **52**, R2253 (1995).
[6] Y. Chikaura, Y. Yoneda, and G. Hildebrandt, J. Appl. Crystallogr. **15**, 48 (1982).
[7] Y. Chikaura, Y. Suzuki, and H. Kii, Jpn. J. Appl. Phys. **33**, L204 (1994).
[8] Y. Chikaura and Y. Suzuki, J. Appl. Crystallogr. **26**, 219 (1993).